Phys Chem Minerals (2003) 30: 620–627
DOI 10.1007/s00269-003-0355-x

ORIGINAL PAPER

R. Zboril · M. Mashlan · K. Barcova
J. Walla · E. Ferrow · P. Martinec

Thermal behaviour of pyrope at 1000 and 1100 °C: mechanism of Fe^{2+} oxidation and decomposition model

Received: 13 March 2003 / Accepted: 14 July 2003

Abstract The mechanism of thermally induced oxidation of Fe^{2+} from natural pyrope has been studied at 1000 and 1100 °C using ^{57}Fe Mössbauer spectroscopy in conjunction with XRD, XRF, AFM, QELS, TG, DTA and electron microprobe analyses. At 1000 °C, the non-destructive oxidation of Fe^{2+} in air includes the partial stabilization of Fe^{3+} in the dodecahedral 24*c* position of the garnet structure and the simultaneous formation of hematite particles (15–20 nm). The incorporation of the magnesium ions to the hematite structure results in the suppression of the Morin transition temperature to below 20 K. The general garnet structure is preserved during the redox process at 1000 °C, in accordance with XRD and DTA data. At 1100 °C, however, oxidative conversion of pyrope to the mixed magnesium aluminium iron oxide, Fe-orthoenstatite and cristoballite was observed. During this destructive decomposition, Fe^{2+} is predominantly oxidized and incorporated into the spinel structure of $Mg(Al,Fe)_2O_4$ and partially stabilized in the structure of orthoenstatite, $(Mg,Fe)SiO_3$. The combination of XRD and Mössbauer data suggest the definite reaction mechanism prevailing, including the refinement of the chemical composition and quantification of the reaction products. The reaction mechanism indicates that the respective distribution of Fe^{2+} and Fe^{3+} to the enstatite and spinel structures is determined by the total content of Fe^{2+} in pyrope.

Keywords Fe-bearing garnet · Mössbauer spectroscopy · Oxidation mechanism · Decomposition products · Alpha Fe_2O_3

R. Zboril (✉) · J. Walla
Department of Inorganic and Physical Chemistry,
Palacky University, Krizkovskeho 10,
771 47 Olomouc, Czech Republic
e-mail: zboril@risc.upol.cz

M. Mashlan
Department of Experimental Physics,
Palacky University, Svobody 26,
771 46 Olomouc, Czech Republic

K. Barcova
Institute of Physics,
Technical University of Ostrava,
Ostrava, Czech Republic

E. Ferrow
Department of Mineralogy and Petrology,
Geological Institute, Lund University,
Sölvegatan 13, 223 62 Lund, Sweden

P. Martinec
Institute of Geonics, Academy of Sciences,
Studentska 1768, 708 00 Ostrava, Czech Republic

Introduction

The thermal behaviour of Fe-bearing garnets in the pyrope–almandine solid solution series is interesting for several reasons. Firstly, these garnets are used in modern technologies, including plasma spraying and high-energy water-jet cutting, and the Fe content and mechanism of the thermal decomposition of these silicates significantly influence their industrial application (Hlavac and Martinec 1998, 1999). Secondly, $(Mg,Fe)SiO_3$ perovskite formed from pyrope–almandine garnets at high temperatures and pressures (Kesson et al. 1995) plays an important role in the formation of mineralogical models of the Earth's lower mantle (McCammon 1997; Hama and Suito 2001; Shim et al. 2001). From industrial and geological viewpoints, therefore, the oxidation and decomposition mechanisms of Fe-bearing garnets are subjects worth studying.

The mechanisms of thermal decomposition of Fe-bearing silicates in the pyrope–almandine series have been poorly investigated. Anovitz et al. (1993) suggested two oxidation mechanisms for a synthetic almandine ($Fe_3Al_2Si_3O_{12}$) with the formation of magnetite, quartz and sillimanite or hercynite, depending on the experimental conditions. According to Zboril et al. (2002a) and Barcova et al. (2001), the thermal oxidation of natural almandine, with the iron content significantly below end-member composition, takes place at about 750 °C following a two-step structural transformation of

maghemite nanoparticles via ε-Fe_2O_3 to hematite. According to Thiéblot et al. (1998), the thermal decomposition of almandine with a chemical composition close to end member begins at about 1000 °C and is triggered by the oxidation of iron, with the formation of hematite, sillimanite and cristoballite. While for the thermal decomposition of a pyrope close to the end member ($Mg_3Al_2Si_3O_{12}$) at temperatures of 1200 °C, corundum and enstatite were identified as the decomposition products. The thermal behaviour of pyrope single crystals was analyzed using X-ray diffraction by Pavese et al. (1995) and neutron diffraction by Artioli et al. (1997); however, these studies provided no information on the decomposition mechanisms, since at temperatures below 900 °C the garnet structure was preserved intact.

In this paper, we will present the findings of a thermal decomposition of garnet with a molar ratio of Mg to Fe close to 2.5 at two temperatures, 1000 and 1100 °C, respectively. We will use ^{57}Fe Mössbauer spectroscopy and X-ray diffraction (XRD) techniques for monitoring the oxidation mechanisms and products of garnet decomposition, because their combination proved to be very effective in studying the oxidation processes and the thermal transformations of Fe-bearing aluminium silicates (Ferrow 1987; Rancourt et al. 2001).

The crystal chemistry of garnets

Garnet is a common name for silicates formed by isolated $(SiO_4)^{4-}$ tetrahedral groups and with a general structural formula given by $X_3Y_2Si_3O_{12}$, where X stands for cations in the dodecahedral 24*c* position ($X = Mg^{2+}$, Ca^{2+}, Fe^{2+}, Mn^{2+}) and Y corresponds to cations in the octahedral 16*a* position ($Y = Al^{3+}$, Fe^{3+}, Cr^{3+}). Natural garnets can be divided into two main subgroups, almandine subgroup (pyralspites) with the end members including pyrope [$Mg_3Al_2Si_3O_{12}$], almandine [$Fe_3Al_2Si_3O_{12}$] and spessartine [$Mn_3Al_2Si_3O_{12}$], and the andradite subgroup (ugrandites) with uvarovite [$Ca_3Cr_2Si_3O_{12}$], grossular [$Ca_3Al_2Si_3O_{12}$] and andradite [$Ca_3Fe_2Si_3O_{12}$] end members. A strong tendency towards isomorphic substitution and the formation of solid solutions are typical for minerals of the garnet group.

Experimental

Red-coloured gem-quality crystals of pyrope, known as a Bohemian garnet, from Podsedice (Czech Republic), were washed with dilute HCl and oxalate acid to remove secondary minerals such as carbonates and Fe-oxyhydroxides. The crystals were rinsed in distilled water and then dried at 100 °C.

The chemical composition and homogeneity of the samples were determined using a 535 M-type Phillips Scanning Electron Microscope, equipped with EDAX 9900 spectrometer. X-ray fluorescence analysis (XRF) was conducted using an Energy Disperse Spectrometer Spectro X-LAB. No chemical zoning or in-homogeneities were observed in the starting garnet crystals. The crystals were then crushed in an agate mill to a powder with a particle size of 1.5–3 μm. The powdered samples of pyrope were isothermally heated at 1000 °C for between 1 and 360 h and at 1100 °C for between 0.5 and 30 h.

The transmission ^{57}Fe Mössbauer spectra of 512 channels were collected using a Mössbauer spectrometer running in constant acceleration mode with a ^{57}Co(Rh) source. Measurements were carried out at temperatures ranging between 12 and 300 K using a cryostat with closed He cycle. The isomer shift values were calibrated using α-Fe foil. The phases produced by decomposition of the garnet grains during the heating experiments were monitored using a Seifert-FPM X-ray spectrometer with CuKα radiation in a conventional θ-2θ geometry. Si was used as an external calibration standard. The atomic force microscopy (AFM) measurements of the selected samples were done in air and at room temperature using the AFM Explorer microscope in a non-contact mode with Si tips of the 1650–00 type at resonant frequencies ranging from 180 to 240 kHz. The particle-size distributions were monitored using the quasi-elastic light-scattering (QELS) method by a 90Plus Particle Sizer Instrument with the MAS OPTION software allowing both the lognormal and the multi modal-size distribution analysis of the powdered systems. Dynamic heat analysis with a simultaneous measurement of differential thermal analysis (DTA) and thermogravimetry (TG) curves was performed in air in a range of 25–1300 °C using an EXSTAR 6000 instrument.

Results and discussion

The chemical formulae of the natural pyrope, as determined using microprobe analysis, can be written as $(Mg_{2.03}Fe_{0.72}Ca_{0.23}Mn_{0.02})(Al_{1.78}Fe_{0.08}Cr_{0.07}Ti_{0.05})Si_3O_{12}$. The Fe^{2+}/Fe^{3+} ratio was determined by Mössbauer spectroscopy.

At room temperature (RT), the Mössbauer spectrum of the initial pyrope could be fitted using two doublets, an asymmetric outer doublet with isomer shift (δ) = 1.28 mm s^{-1} and quadrupole splitting (ΔE_Q) = 3.54 mm s^{-1} and a symmetric inner doublet with $\delta = 0.23$ mm s^{-1} and $\Delta E_Q = 0.38$ mm s^{-1} (Fig. 1). The

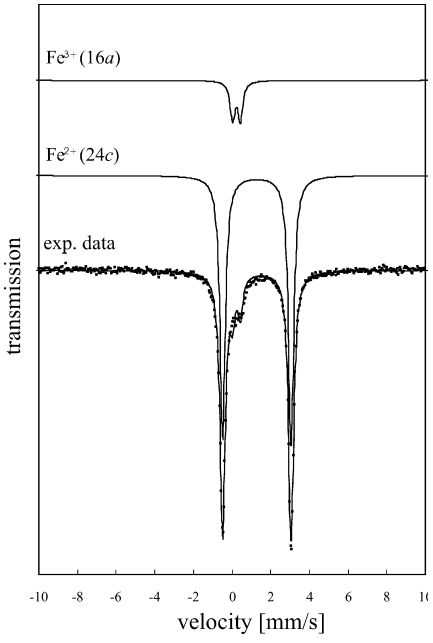

Fig. 1 RT Mössbauer spectrum of the the pyrope used as a starting material in the heating experiments

former doublet is assigned to Fe^{2+} in the 24*c* site and the latter to Fe^{3+} in the 16*a* site of the pyrope structure. The asymmetry of the Fe^{2+} doublet is commonly observed in the RT Mössbauer spectra of Fe-bearing pyropes and can be explained as arising out of a paramagnetic relaxation of Fe^{2+} in the dodecahedral position (Amthauer et al. 1976; Murad and Wagner 1987; Mitra 1992) or by the Goldanskii–Karyagin effect (Geiger et al. 1992). The XRD pattern shows lines exclusively corresponding to the cubic pyrope structure with lattice parameter $a_0 = 1.1480(10)$ nm and with no indications of the presence of other phases.

For the initial information on the thermal stability and transformation mechanism of pyrope, a TG and DTA thermal analysis was done in air with a temperature increase of 1 °C min^{-1} at temperature intervals of 25 to 1300 °C. The TG curve reveals a slight increase in weight (1.2%) at 990 °C, probably related to the beginning air oxidation of Fe^{2+}. The final mass increase, recorded at 1300 °C, totals 2.7%. The slow oxidation of Fe^{2+} in the pyrope structure is manifested by a weak exothermic peak at 1020 °C in the DTA curve. The more intensive endothermic peak at 1125 °C indicates the decomposition of the garnet structure following the oxidation of structural Fe.

In order to better understand the oxidation and decomposition mechanisms involved when garnet is heated in air, the samples were isothermally heated at 1000 and 1100 °C for different periods of time and were analyzed using Mössbauer spectroscopy and XRD.

The Mössbauer parameters for the different runs heated at 1000 °C are presented in Table 1 and the RT Mössbauer spectrum of the sample heated for 120 h, taken as a representative spectrum for the whole series, is plotted in Fig. 2. Table 1 and Figure 2 show the presence of four non-equivalent Fe sites in samples heated at

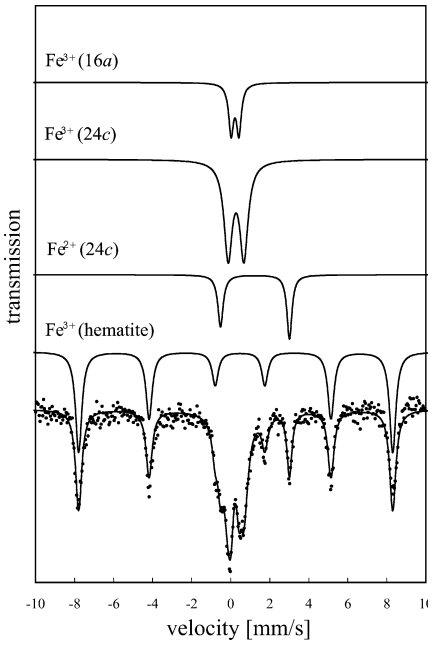

Fig. 2 RT Mössbauer spectrum of pyrope heated at 1000 °C for 120 h

1000 °C. The first two correspond to Fe^{2+} in the dodecahedral 24*c* position and Fe^{3+} in the octahedral 16*a* site of the pyrope structure. The Mössbauer parameters are similar to those observed in Fig. 1 for the thermally untreated sample. Note that while the spectral area of Fe^{2+} in the dodecahedral 24*c* position decreases with time, the spectral area of Fe^{3+} in the 16*a* site remains constant.

The new paramagnetic doublet observed when pyrope is oxidized has δ slightly higher than that of Fe^{3+} in the 16*a* site but with ΔE_Q nearly twice as large,

Table 1 RT Mössbauer spectra parameters of pyrope heated in air at 1000 °C for different periods of time

Fe phase	Parameter	1 h	3 h	15 h	120 h	360 h
Fe^{2+} (24c-pyrope)	δ[a] (mm s^{-1})	1.27	1.27	1.27	1.26	1.26
	ΔE_Q[b] (mm s^{-1})	3.53	3.53	3.53	3.51	3.50
	Γ (mm s^{-1})	0.32	0.31	0.29	0.34	0.34
	RA (%)	65.8	62.5	48.1	11.5	3.2
Fe^{3+} (16a-pyrope)	δ (mm s^{-1})	0.22	0.23	0.24	0.24	0.22
	ΔE_Q (mm s^{-1})	0.35	0.34	0.38	0.38	0.39
	Γ (mm s^{-1})	0.29	0.30	0.30	0.30	0.29
	RA (%)	9.5	9.8	9.8	9.1	9.3
Fe^{3+} (24c-pyrope)	δ (mm s^{-1})	0.27	0.27	0.28	0.26	0.26
	ΔE_Q (mm $s^{-1)}$	0.75	0.76	0.75	0.79	0.78
	Γ (mm s^{-1})	0.50	0.47	0.50	0.52	0.51
	RA (%)	11.7	12.3	18.0	32.8	36.8
Fe^{3+} (hematite)	δ (mm s^{-1})	0.36	0.35	0.37	0.37	0.38
	ε (mm s^{-1})	−0.22	−0.23	−0.22	−0.22	−0.21
	B[c] (T)	50.5	50.3	50.4	49.9	50.3
	Γ (mm s^{-1})	0.38	0.39	0.37	0.38	0.44
	RA[d] (%)	13.0	15.4	24.1	46.6	50.7

[a] δ isomer shift
[b] $\Delta E_Q(\varepsilon)$ quadrupole splitting (shift)
[c] *B* hyperfine magnetic field
[d] RA relative area

reflecting a lower symmetry of the Fe environment. The site was assigned, therefore, to Fe^{3+} ions in the dodecahedral 24*c* position (Novak and Gibbs 1971). Its increasing spectral area with heating time indicates the gradual oxidation of Fe^{2+} in the 24*c* position.

The only magnetically ordered component in the RT Mössbauer spectra of pyrope samples thermally treated at 1000 °C presents hyperfine parameters that correspond well with those of hematite (Table 1). Its relative area increases with time, as in the case of Fe^{3+} ions in the 24*c* position. It seems that the thermally induced oxidation of Fe^{2+} in air results in the partial stabilization of Fe^{3+} in the 24*c* position of the pyrope structure and in the incorporation of the redundant Fe^{3+} in the hematite. In this redox system, hematite serves as the compensator of the change in charge of Fe atoms in the 24*c* position as well as the host for the oxygen reduced, as represented by Eq (1). The oxidation mechanism at 1000 °C can be clearly demonstrated using the time dependence of the spectral relative areas corresponding to non-equivalent Fe components in Mössbauer spectra (Fig. 3).

$$6Fe^{2+}(24c) + 3/2O_2 \rightarrow 4Fe^{3+}(24c) + \alpha\text{-}Fe_2O_3 \ . \qquad (1)$$

Barcova et al. (2001) reported the presence of superparamagnetic nanoparticles of Fe^{3+} oxide when almandine was oxidized in air at 750 °C. It is possible that the doublet assigned to Fe^{3+} in the 24*c* site in this study could correspond to Fe^{3+} oxide in superparamagnetic state as well. Mössbauer measurements taken at 20 K for the sample heated to 120 h (Fig. 4), however, show that the site remains paramagnetic at low temperature and, moreover, its isomer shift is significantly lower than is the case for hematite and other ferric oxides at the corresponding temperature (Zboril et al. 2002b).

There are additional aspects in this study that are interesting from the viewpoint of the transformation mechanism at 1000 °C. Firstly, the low value of the quadrupole shift parameter of hematite at 20 K indicates its weakly ferromagnetic ordering, similar to the observation made at room temperature, although a Morin temperature of the magnetic transition from weakly ferromagnetic to antiferromagnetic state is usually reported at about 260 K (Kvardakov et al. 1991). Such a drastic reduction of the Morin temperature in this study could be related either to the considerable substitution of aluminium in the hematite structure (Van San et al. 2001) or to the very low crystallinity of the hematite particles formed (Sahu et al. 1997). In order to understand the reasons behind the low Morin transition temperature observed, the hematite particles were separated from the sample heated at 1000 °C for 360 h by the sedimentation method (Zboril et al. 2002a) and analyzed using AFM, QELS and XRF.

As Fig. 5 shows, the AFM image of the hematite particles reveals a narrow size range, 15 to 25 nm, and almost spherical morphology, with the ratio of the

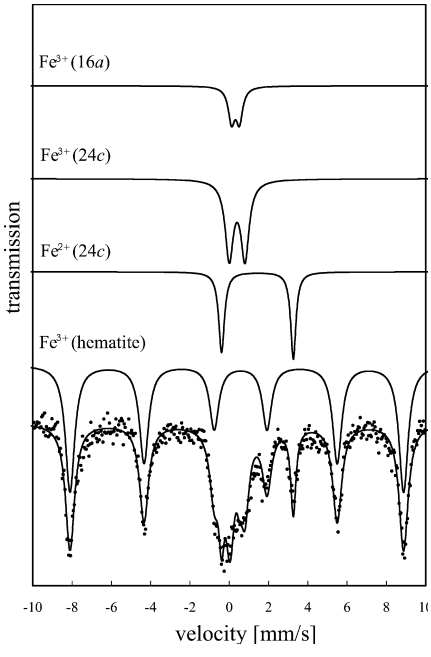

Fig. 4 (20 K) Mössbauer spectrum of pyrope heated at 1000 °C for 120 h

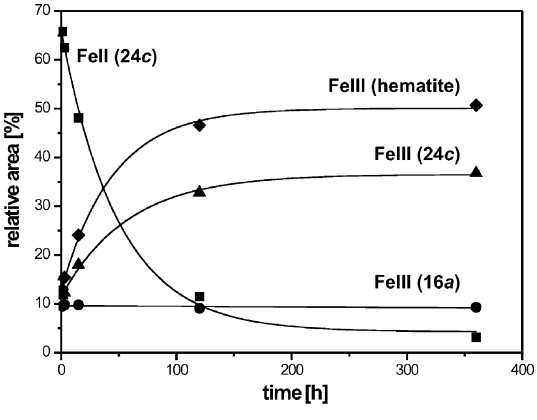

Fig. 3 Time behaviour of the spectral relative areas at 1000 °C

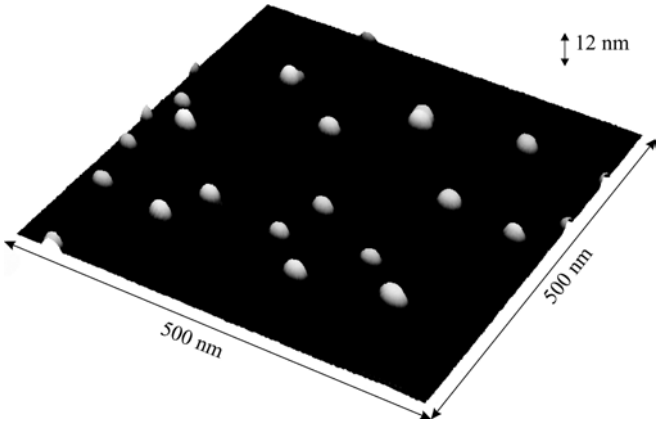

Fig. 5 AFM image of hematite particles formed during the oxidation of pyrope at 1000 °C

lateral to the vertical dimension close to 1.3. Similarly, the quasi-elastic light-scattering method indicates a lognormal particle-size distribution with a mean diameter of 21 nm. The narrow size distribution and the generally small size of the hematite particles show evidence of their poor agglomeration during the thermal treatment at 1000 °C. Surprising limitation of the sintering process at such a high temperature cannot be explained by the formation of a composite Fe oxide mineral, as in the case of aluminosilicates with a porous structure (Bourlinos et al. 2003). In the hematite–pyrope system, ultrafine particles of hematite can be protected from sintering by their low weight concentration or by the cation substitution in their structure.

The low crystallinity of hematite particles observed indeed contributes to the reduction of the Morin transition temperature. However, for hematite particles with slightly larger size (29 nm), Vandenberghe et al. (2002) determined a Morin transition temperature close to 211 K. In this study, therefore, the drastic decrease in Morin transition temperature to below 20 K cannot be attributed to the particle-size effect alone.

Taking into account the high probability that cation substitution may be affecting the low Morin transition temperature observed, XRF analysis of the separated hematite sample was performed. The analysis shows Mg content as high as 0.82 wt%, while the contents of the other elements including aluminium were found to be lower than 0.01 wt%. The result accords with the redox mechanism suggested in Eq. (1), where the hematite structure is formed by Fe atoms originating from the reactive 24*c* site of the garnet structure. The significant content of Mg in the 24*c* site can result in partial extraction from the pyrope structure and its incorporation into the hematite structure. As a result, a slight substitution of Mg is enough for significant reduction of the Morin transition temperature in hematite.

The most interesting fact related with the transformation mechanism at 1000 °C is the non-destructive character of the oxidation process. The almost complete oxidation of Fe^{2+} in the 24*c* position, their partial extraction from the pyrope structure and transformation to hematite does not result in the complete decomposition of the garnet structure, in accordance with XRD data. XRD patterns of the initial powdered pyrope and the pyrope heated at 1000 °C for 360 h differ particularly by the presence of the additional lines of hematite in the heated sample. Nevertheless, the positions of the lines corresponding to the garnet structure and the refined lattice parameters confirm the decrease of the cell dimension after oxidation in the 24*c* position.

The Mössbauer parameters for the different runs heated at 1100 °C are presented in Table 2 and the representative RT Mössbauer spectrum of the sample heated for 3 h is plotted in Fig. 6. As Table 2 and Fig. 6 show, at 1100 °C the transformation mechanism changes significantly and new Fe phases appear in the RT Mössbauer spectra of thermally treated pyrope samples.

In addition to the hematite lines, two Fe^{2+} doublets and a broad Fe^{3+} doublet are revealed in the RT Mössbauer spectra of the products of thermal treatment of pyrope at 1100 °C. In the samples heated for 1–15 h, powder diffraction analysis show that Fe-orthoenstatite, Fe-spinel, cristoballite and hematite were identified as the decomposition products. Using the XRD data, the two Fe^{2+} doublets can easily be attributed to Fe^{2+} at

Table 2 RT Mössbauer spectra parameters of pyrope heated in air at 1100 °C for different periods of time. Explanations as in Table 1

Fe phase	Parameter	0.5 h	1 h	3 h	15 h	30 h
Fe^{2+} (24c-pyrope)	δ (mm s^{-1})	1.27	1.27	1.27	–	–
	ΔE_Q (mm s^{-1})	3.52	3.51	3.54	–	–
	Γ (mm s^{-1})	0.28	0.28	0.29	–	–
	RA (%)	53.1	27.6	11.1	–	–
Fe^{3+} (16a-pyrope)	δ (mm s^{-1})	0.23	0.23	–	–	–
	ΔE_Q (mm s^{-1})	0.37	0.36	–	–	–
	Γ (mm s^{-1})	0.31	0.30	–	–	–
	RA (%)	6.1	3.1	–	–	–
Fe^{2+} (M1-enstatite)	δ (mm s^{-1})	1.21	1.20	1.19	1.21	–
	ΔE_Q (mm s^{-1})	2.40	2.38	2.38	2.41	–
	Γ (mm s^{-1})	0.32	0.32	0.30	0.30	–
	RA (%)	4.8	6.1	7.4	3.7	–
Fe^{2+} (M2-enstatite)	δ (mm s^{-1})	1.08	1.10	1.11	1.10	–
	ΔE_Q (mm s^{-1})	2.02	2.06	2.06	2.09	–
	Γ (mm s^{-1})	0.31	0.32	0.32	0.31	–
	RA (%)	3.2	4.5	5.3	2.4	–
Fe^{3+} (spinel)	δ (mm s^{-1})	0.33	0.34	0.33	0.33	0.33
	ΔE_Q (mm s^{-1})	0.85	0.86	0.83	0.83	0.85
	Γ (mm s^{-1})	0.57	0.58	0.58	0.56	0.56
	RA (%)	32.8	55.7	71.2	81.1	81.0
Fe^{3+} (hematite)	δ (mm s^{-1})	–	0.36	0.37	0.37	0.36
	ε (mm s^{-1})	–	−0.19	−0.22	−0.22	−0.22
	B (T)	–	50.8	50.6	50.7	50.7
	Γ (mm s^{-1})	–	0.42	0.42	0.44	0.46
	RA (%)	–	3.0	5.0	12.8	19.0

the non-equivalent M1 and M2 sites of the pyroxene structure. The Mössbauer parameters obtained confirm the assignment proposed by Srivastava (1987) for the RT Mössbauer spectrum of orthoenstatite with low iron content. Following Marshall and Dollase (1984), the dominant Fe^{3+} doublet is assigned to Fe^{3+} ions in the spinel structure of $Mg(Al,Fe)_2O_4$.

After 15 h of the thermal treatment, XRD analysis shows the complete decomposition of the garnet structure as documented by the absence of the lines belonging to the original pyrope and the presence of lines that belong to the above-mentioned decomposition products (Fig. 7).

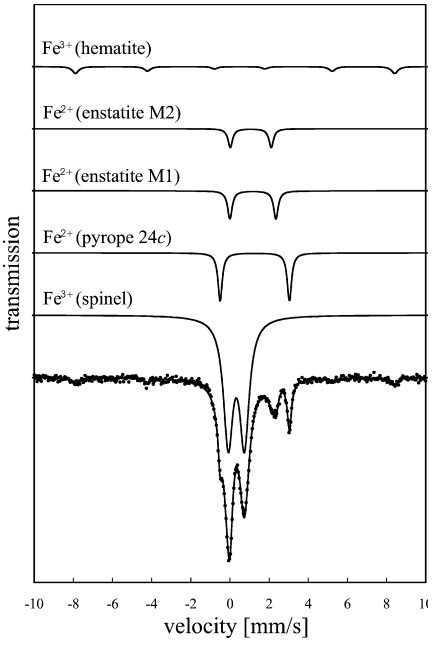

Fig. 6 RT Mössbauer spectrum of pyrope heated at 1100 °C for 3 h

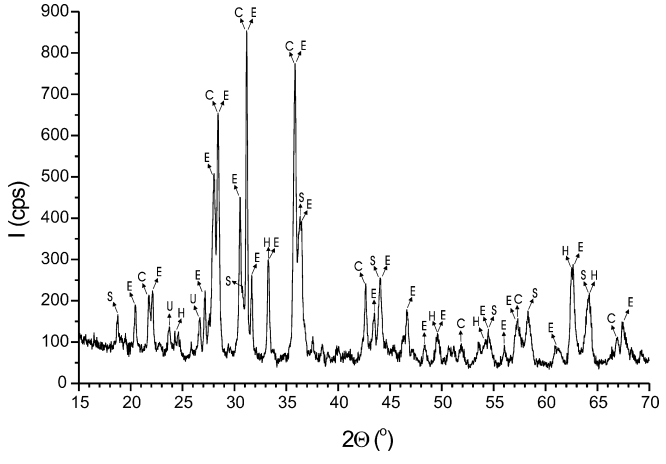

Fig. 7 XRD pattern of pyrope heated at 1100 °C for 15 h with the assignment of the dominant lines. *E* enstatite; *S* spinel; *C* cristoballite; *H* hematite; *U* unidentified

As Table 2 shows, the changes in the spectral areas with heating time allow one to monitor the mechanism of decomposition prevailing at 1100 °C.

The Fe^{3+} doublet assigned to $Mg(Al,Fe)_2O_4$ appears immediately as the dominant product soon after heating the sample for 0.5 h and its relative area increases until the garnet structure has been completely decomposed after 15 h of heating. After the garnet structure has been fully decomposed, the relative area corresponding to $Mg(Al,Fe)_2O_4$ remains constant, reflecting the thermal stability of the spinel structure. The Fe-bearing orthoenstatite, represented by the two doublets, is formed simultaneously with the spinel as the primary decomposition phase after heating the garnet for 0.5 h. Its amount increases as heating progresses and reaches a maximum value after 3 h of heating and then decreases until it totally disappears after 15 h of heating. Hematite, as a secondary oxidation phase, appears first in the Mössbauer spectrum of the sample after heating for 1 h and its content increases gradually as the heating progresses. After the complete decomposition of the garnet structure, the increase in hematite content corresponds to the simultaneous decrease of Fe^{2+} in Fe-orthoenstatite (Table 2).

On the basis of the obtained XRD and Mössbauer data, the primary oxidative decomposition of the garnet structure resulting in the formation of spinel, pyroxene and cristoballite can be summarized by the equation below:

$$X_{3-x_1}\mathrm{Fe}^{\mathrm{II}}_{x_1}Y_{2-x_2}\mathrm{Fe}^{\mathrm{III}}_{x_2}\mathrm{Si_3O_{12}} + a\mathrm{O_2} \rightarrow bXY_{2-(y+x_2)}\mathrm{Fe}^{\mathrm{III}}_{y+x_2}\mathrm{O_4} + cX_{1-z}\mathrm{Fe}^{\mathrm{II}}_{z}\mathrm{SiO_3} + d\mathrm{SiO_2}\ , \quad (2)$$

where a, b, c, d and x_1, x_2, y, z are the stoichiometric coefficients and X stands for cations other than Fe^{2+}, mostly Mg, in the 24*c* position and Y stands for cations other than Fe^{3+}, mostly Al, in the 16*a* position.

In the second oxidation stage, Fe^{2+} from enstatite is oxidized to hematite as typical for oxidation mechanism of Mg-rich orthopyroxenes (Straub et al. 1991). The constant ratio of the spectral area of spinel to the sum of spectral areas of enstatite and hematite $\mathrm{Fe}^{3+}_{\mathrm{spinel}}/(\sum_{\mathrm{M1,M2}}\mathrm{Fe}^{2+}_{\mathrm{enstatite}}+\mathrm{Fe}^{3+}_{\mathrm{hematite}})$ is close to 4 (Table 2), supports the two-step oxidation model suggested and confirms the subsequent exchange of Fe atoms between enstatite and hematite.

The general mechanism represented in Eq. (2) can be refined and all the stoichiometric coefficients can be determined on the basis of the mass balance for individual elements in combination with the experimental data. From the mass balance for Mg, Al, Fe, Si and O, the following equations can be derived:

$$3 - x_1 = b + c(1 - z)\ , \quad (3)$$

$$2 - x_2 = b[2 - (y + x_2)]\ , \quad (4)$$

$$x_1 + x_2 = b(y + x_2) + cz\ , \quad (5)$$

$$3 = c + d \quad , \tag{6}$$

$$12 + 2a = 4b + 3c + 2d \quad . \tag{7}$$

The coefficients x_1 and x_2 can be determined from the chemical analysis of the starting material as determined by electron microprobe analysis, XRF and Mössbauer spectroscopy. Thus, there are six unknowns and five equations left. The last equation and the refinement of Eq. (2), taking into account the non-parametric solution of the system of equations, can be obtained from the Mössbauer analysis of the corresponding spectral areas in the fully decomposed pyrope. For example, we can easily determine k, the ratio of ferric ions incorporated into the structure of the spinel to the overall number of iron ions in the system by:

$$k = \frac{b(y + x_2)}{x_1 + x_2} \quad . \tag{8}$$

By solving the system of Eq. (3) to (8) and if the trace elements in X and Y replacing Mg and Al are neglected, then the refined oxidation mechanism at 1100 °C can be formulated by:

$$\begin{aligned} &Mg_{2.28}Fe^{II}_{0.72}Al_{1.92}Fe^{III}_{0.08}Si_3O_{12} + 0.14O_2 \\ &\quad \rightarrow 1.28MgAl_{1.5}Fe^{III}_{0.5}O_4 + 1.15Mg_{0.87}Fe^{II}_{0.13}SiO_3 \\ &\quad + 1.85SiO_2 \quad . \end{aligned} \tag{9}$$

All the coefficients are given after rounding off the two decimal positions. The decomposition mechanism suggested in Eq. (2) probably has a general character. Evidently, the enormous decrease in the Fe^{2+} content (the shift of the chemical composition to the end-member $Mg_3Al_2Si_3O_{12}$) results in the decomposition to enstatite and corundum and the former is probably the host compound for the traces of Fe^{2+} left (Thiéblot et al 1998).

Conclusion

Two completely different mechanisms were found prevailing for thermally induced oxidation of Fe^{2+} in pyrope in air; one conserves the garnet structure, the other destroys it. Heating pyrope at 1000 °C involves the oxidation of Fe^{2+} in the 24*c* position accompanied by the formation of Mg-substituted hematite nanoparticles with the garnet structure still preserved. Heating at 1100 °C occurs in two steps, resulting in the formation of two thermally stable Fe^{3+}-bearing oxides and the breakdown of the garnet structure. The primary oxidation phase, $Mg(Al,Fe)_2O_4$, forms directly during the oxidative decomposition of the garnet structure. Hematite forms at 1100 °C as a product of the subsequent oxidation of Fe^{2+} from enstatite.

The validity of these oxidation and decomposition mechanisms for other natural pyropes can be determined only on the basis of the experimental study of thermal behaviour of garnets with varying Fe contents, a study currently in progress in our laboratory.

Acknowledgements Financial support from the Grant Agency of the Czech Republic under projects 202/00/0982, 202/00/D091 is gratefully acknowledged.

References

Amthauer G, Annersten H, Hafner SS (1976) The Mössbauer spectrum of ^{57}Fe in silicate garnets. Z Kristallogr 143: 14–55

Anovitz LM, Essene EJ, Metz GW, Bohlen SR, Westrum EF, Hemingway BS (1993) Heat capacity and phase equilibria of almandine, $Fe_3Al_2Si_3O_{12}$. Geochim Cosmochim Acta 57: 4191–4204

Artioli G, Pavese A, McMullan RK (1997) Single-crystal neutron-diffraction study of pyrope in the temperature range 30–1173 K. Can Mineral 35: 1009–1019

Barcova K, Mashlan M, Zboril R, Martinec P, Kula P (2001) Thermal decomposition of almandine garnet – Mössbauer study. Czech J Phys 51: 749–754

Bourlinos AB, Zboril R, Petridis D (2003) A simple route towards magnetically modified zeolites. Micropor Mesopor Mat 58: 155–162

Ferrow E (1987) Mössbauer and X-ray studies on the oxidation of annite and ferriannite. Phys Chem Miner 14: 270–275

Geiger CA, Armbruster T, Lager GA, Jiang K, Lottermoser W, Amthauer G (1992) A combined temperature-dependent ^{57}Fe Mössbauer and single-crystal X-ray diffraction study of synthetic almandine – evidence for the Goldanskii–Karyagin effect. Phys Chem Miner 19: 121–126

Hama J, Suito K (2001) Thermoelastic models of minerals and the composition of the Earth's lower mantle. Phys Earth Planet In 125: 147–166

Hlavac L, Martinec P (1998) Almandine garnets as abrasive material in high-energy water jet – physical modeling of interaction, experiments and prediction. In: Proceedings 14th International Conference on Jetting Technology. BHR Group, Prof. Eng. Pub. Ltd, London, pp 211–223

Hlavac L, Martinec P (1999) Abrasives for high-energy water jet: investigation of properties. In: Hashish M (ed) Proceedings 10th American Water Jet Conference. Water Jet Technology Association, St. Louis, Houston, pp 409–418

Kesson SE, Gerald JDF, Shelley JMG, Withers RL (1995) Phase relations and crystal chemistry of some aluminous silicate perovskites. Earth Planet Sci Lett 134: 187–201

Kvardakov VV, Sandonis J, Podurets KM, Shilstein SSh, Baruchel J (1991) Study of the Morin transition in nearly perfect crystals of hematite by diffraction and topography. Physica (B) 168: 242–250

Marshall I, Dollase W (1984) Cation arrangement in Fe–Zn–Cr spinel oxides. Am Mineral 69: 928–936

McCammon C (1997) Perovskite as a possible sink for ferric iron in the lower mantle. Nature 387: 694–696

Mitra S (1992) Applied Mössbauer spectroscopy. Pergamon, Oxford, pp. 137–138

Murad E, Wagner FE (1987) The Mössbauer spectrum of almandine. Phys Chem Miner 14: 264–269

Novak GA, Gibbs GV (1971) The crystal chemistry of the silicate garnets. Am Mineral 56: 791–825

Pavese A, Artioli G, Prencipe M (1995) X-ray single-crystal diffraction study of pyrope in the temperature range 30–973 K. Am Mineral 80: 457–464

Rancourt DG, Mercier PHJ, Cherniak DJ, Desgreniers S, Kodama H, Robert JL, Murad E (2001) Mechanisms and crystal chemistry of oxidation in annite: resolving the hydrogen-loss and vacancy reactions. Clay Clay Miner 49: 455–491

Sahu KK, Rath C, Mishra NC, Anand S, Das RP (1997) Microstructural and magnetic studies on hydrothermally prepared hematite. J Colloid Interf Sci 185: 402–410

Shim SH, Duffy TS, Shen GY (2001) Stability and structure of $MgSiO_3$ perovskite to 2300-kilometer depth in Earth's mantle. Science 293: 2437–2440

Srivastava KKP (1987) Mössbauer study of spin–spin relaxation of Fe(II) ions in natural orthopyroxenes. J Phys (C)-Solid State Phys 20: 2161–2168

Straub DW, Burns RG, Pratt SF (1991) Spectral signature of oxidized pyroxenes – implications to remote sensing of terrestrial planets. J Geophys Res 96: 18819–18830

Thiéblot L, Roux J, Richet P (1998) High - temperature thermal expansion and decomposition of garnets. Eur J Mineral 10: 7–15

Vandenberghe RE, Van San E, de Grave E, da Costa GM (2001) About the Morin transition in hematite in relation with particle size and aluminum substitution. Czech J Phys 51: 663–675

Van San E, De Grave E, Vandenberghe RE, Desseyn HO, Datas L, Barron V, Rousset A (2001) Study of Al-substituted hematites, prepared from thermal treatment of lepidocrocite. Phys Chem Miner 28: 488–497

Zboril R, Mashlan M, Barcova K, Vujtek M (2002a) Thermally induced solid-state syntheses of γ-Fe_2O_3 nanoparticles and their transformation to α-Fe_2O_3 via ε-Fe_2O_3. Hyperfine Interact 120–121: 497–501

Zboril R, Mashlan M, Petridis D (2002b) Iron(III) oxides from thermal processes – synthesis, structural and magnetic properties, Mössbauer spectroscopy characterization, and applications. Chem Mater 14: 969–982